Journal of Non-Crystalline Solids 68 (1984) 301–325
North-Holland, Amsterdam

THERMAL BLEACHING OF X-RAY-INDUCED DEFECT CENTERS IN HIGH PURITY FUSED SILICA BY DIFFUSION OF RADIOLYTIC MOLECULAR HYDROGEN

David L. GRISCOM

Naval Research Laboratory, Washington, DC 20375, USA

Received 30 November 1983

High purity Type-III fused silicas (1200 ppm OH) were subjected to 100 keV X-irradiation at 77 K and investigated by electron spin resonance (ESR) before and after heat treatments to higher temperatures. Theoretical fits to the isochronal and isothermal anneal curves of the nonbridging oxygen hole center (OHC) have been accomplished using Waite's equation for diffusion-limited bimolecular recombination in solids under the working hypothesis that the diffusing species is radiolytic molecular hydrogen. The analysis supports the notion that there exists a statistical distribution in activation energies for H_2 diffusion in amorphous SiO_2, and percolation theory is invoked to explain the generally lower activation energies measured in the present experiment vis-à-vis the results of more classical gas evolution studies. The occurrence of molecular hydrogen as a product of radiolysis in high-OH Type-III silicas appears to provide a natural radiation-protection mechanism (room temperature fading) which might be inadvertently thwarted by heat treatments which drive out hydrogen prior to irradiation. The significance of these results in the fiber optic context is emphasized.

1. Introduction

It has long been known that high purity amorphous silica (a-SiO_2) is neglibibly colored by intensive X-irradiation at room temperature [1–3], whereas fast neutrons produce UV coloration [4] and paramagnetic defect populations [5] which grow with increasing dose, saturate at very high levels, and remain indefinitely stable at 300 K. Arnold and Compton [2,3] noted, however, that X-irradiation at $\lesssim 77$ K results in induced UV absorptions at 215 and 257 nm which are 10 times or more as intense as the corresponding absorptions induced by the same exposure at room temperature. These bands were observed to bleach slowly when the sample temperature was subsequently raised to 300 K [2,3].

More recently, analogous results have been obtained for pure-silica-core fiber optic waveguides exposed to γ ray doses of $\lesssim 10^6$ rad [6–10]. In these measurements the absorption has been studied in the visible-IR range ($\sim$ 0.5–1.7 μm) where the induced absorption coefficients are orders of magnitude lower than in the UV but easily observable in the fiber optic geometry. Again, higher induced absorptions are recorded at lower temperatures and slow

thermal bleaching is observed in the temperature range near and above 300 K [8–10].

The mechanisms by which defects in high purity a-SiO_2 are thermally bleached have never been thoroughly delineated. The popular wisdom over the years has tended to hold that the trapped electrons and holes responsible for the optical absorptions recombine after one of these species or the other is thermally detrapped and diffuses through the conduction or valence bands to the site of its complement (e.g. ref. [11]). Recently, however, Edwards and Fowler [12] have made a case for an alternative mechanism based on the diffusion of small molecules. These authors specifically discussed the annealing of E′ centers in γ-irradiated low-OH silicas by O_2 diffusion. Since in this particular case (γ-ray doses $\gg 10^6$ rad, OH concent $\lesssim 2$ ppm) the temperature required for thermal bleaching is $\sim 200\,^{\circ}C$ [13], the O_2-diffusion mechanism cannot explain the room-temperature fading observed in high-OH samples which are X-irradiated or subject to γ-ray doses $\lesssim 10^6$ rad.

Revesz [14] has given one of the earlier discussions of the possible roles of atomic or molecular hydrogen in the radiolysis of amorphous silica containing OH groups (a-SiO_2 : OH). In particular, the reaction

$$\equiv \mathrm{Si{-}OH} \rightleftharpoons \equiv \mathrm{Si{-}O^{\cdot}} + \mathrm{H}^{\circ} \qquad (1)$$

was seen as proceeding to the right upon irradiation and to the left upon thermal annealing. Subsequently, Silin, Skuya and Shendrik [15,16] demonstrated these processes in high-OH silicas X-irradiated at 80 K by monitoring the 630 nm (red) photoluminescence which they were able to associate with the nonbridging oxygen hole center ($\equiv$ Si–O·). (For simplicity, the nonbridging oxygen hole center will be referred to simply as the "OHC" in the remainder of this paper.) Silin and Skuya [16] noted that a decrease in the induced red luminescence between 80 and 130 K coincides with the disappearance of the well known electron spin resonance (ESR) doublet due to atomic hydrogen. They were able to fit their isochronal anneal data for the red luminescence intensity to the diffusion-limited reverse reaction of eq. (1) with an activation energy of 0.07 eV for H° diffusion. A second-stage decrease in the luminescence above ~ 200 K evident in their data was not explained in ref. [16].

Very recently, Griscom et al. [17] have performed an extensive series of ESR experiments on Type-III (1200 ppm OH) silicas subjected to 100 keV X-irradiation at 77 K and measured at 100 K. In several ways, this work shed additional light on the mechanisms by which the induced defect centers thermally bleach. First, all of the paramagnetic defects intrinsic to the system a-SiO_2 : OH were measured *directly* by ESR and quantified in spins per gram as functions of anneal time and temperature. These defects included H°, the OHC [13], and the E′ center [18–21]. Second, the discovery and characterization of an unexpected *extrinsic* defect, the formyl radical, demonstrated for the first time the existence and role of radiolytic molecular hydrogen in the X-ray radiolysis of a-SiO_2 : OH (see additional discussion in section 2).

Here, a clear distinction is to be drawn between *radiolytic* molecular

hydrogen – which is argued to be an "intrinsic defect" in irradiated a-SiO_2 : OH [17] – and dissolved "excess" H_2, which has been shown by Faile and Roy [22,23] to suppress the formation of the usual defect centers upon irradiation. Hartwig [24], Shelby and coworkers [25,26], and Vitko [27] have also studied radiation effects in such hydrogen-impregnated silicas, and their results should ultimately provide additional insights on the mechanisms of radiation damage in normal, untreated a-SiO_2 : OH. In this context, mention should be made also of the demonstration by Shelby [28] of "chemical annealing" of defects in low-OH Type I silicas by H_2 permeation following irradiation.

The purpose of the present paper is to apply bimolecular reaction rate theory [29] in an analysis of the isochronal and isothermal anneal kinetics of the OHC as induced by X-rays at 77 K. The central premise of this work is that the second-stage bleaching of the OHC found to occur near 230 K [16,17] is due to the diffusion-limited reaction [17]

$$\equiv \mathrm{Si{-}O^{\cdot}} + \mathrm{H_2} \overset{230\ \mathrm{K}}{\rightarrow} \equiv \mathrm{Si{-}OH} + \mathrm{H^{\circ}}, \tag{2}$$

where the molecular hydrogen in eq. (2) is *radiolytic*, resulting from the dimerization of some of the atomic hydrogen produced in eq. (1). That the reaction of eq. (2) should in fact be limited by diffusion, rather than reaction, can be inferred from data for the analogous process

$$\mathrm{{}^{\cdot}OH} + \mathrm{H_2} \rightarrow \mathrm{H_2O} + \mathrm{H^{\circ}}. \tag{3}$$

(Note that $\equiv$ Si–O$^{\cdot}$ and $^{\cdot}$OH are both free radicals having essentially identical electronic structure surrounding the oxygen.) The preferred rate constant for eq. (3) is tabulated as $R = 1.8 \times 10^{-11} \exp[-2330/T]$ cm^3 mol.$^{-1}$ s^{-1}, valid to temperatures as low as 210 K [30]. The value of R calculated for $T = 230$ K (7.2×10^{-16} cm^3 mol.$^{-1}$ s^{-1}) is substantially more rapid than the diffusion-limited rate $4\pi r^* D$ (2.4×10^{-20} cm^3 mol.$^{-1}$ s^{-1}) calculated for the same temperature using the diffusion coefficient D for H_2 in silica glass given by Lee [31] and assuming a capture radius r^* of 5 Å (see Section 3).

2. The Experiment

Fig. 1 epitomizes a larger set of isochronal anneal data presented in ref. [17] for previously unirradiated, manufacturer's stock 4 mm-diameter rods of Type III fused silicas. The particular samples of fig. 1 were Suprasil 1, and the 100 keV X-ray dose administered at 77 K was 1.5×10^6 rad (Si). Each data point represents a five minute *in situ* anneal, performed in ascending order, and remeasurement at 100 K. Spin concentrations were determined by numerical integrations of the ESR spectra and comparison with a Varian "strong pitch" standard.

Four generic defect types are identified in the figure: H°, E'_β, OHC, and the formyl radical. E'_β is a particular variation of the usual E′ center which is

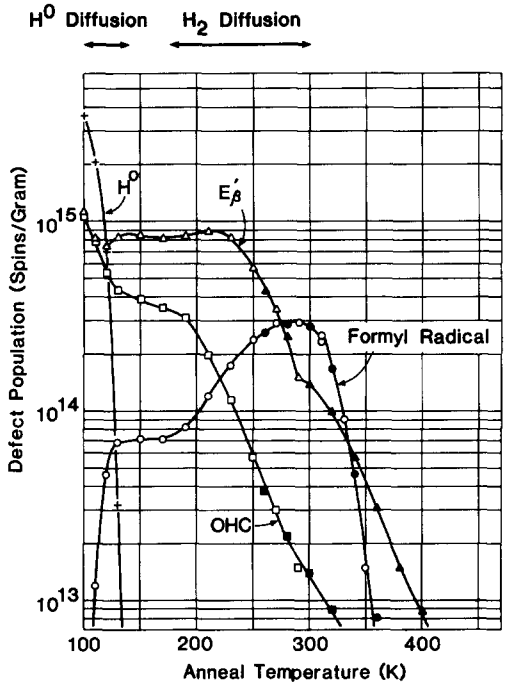

Fig. 1. Isochronal anneal curves for 100 keV X-ray induced defects in Suprasil 1 (open and filled symbols represent two separate samples). ESR spectra were recorded at 100 K following X-irradiation to a dose of 1.5×10^6 rad at 77 K and five-minute pulse anneals at the indicated temperatures. Spectroscopic identifications of the various defect centers have been described elsewhere [13,17,21]. Temperature regimes wherein defect anneal processes are ascribed to H° or H_2 diffusion are delineated by horizontal arrows at the top (see text). (Figure adapted from ref. [17].)

distinguished from the others by its relatively more axial g matrix [21] and by its production mechanism. This mechanism has been inferred from the growth of E'_β comcomitant with the decay of H° near 130 K [17]:

$$\left(E'_\beta \text{ precursor}\right) + H^\circ \rightarrow E'_\beta + H^+ . \tag{4}$$

As with all E′ centers, the unpaired spin of E'_β has been shown [21] to be localized in a dangling tetrahedral orbital of a silicon bonded to only three oxygens in the glass network. The fate of the proton on the righthand side of eq. (4) is not known from the experiment beyond the fact that E'_β does not exhibit a measurable proton hyperfine splitting [17]. *

* It is still conceivable that the proton remains incorporated in the overall structure of the E'_β center (see section 8). However, the mean distance between any proton and the unpaired electron spin can be calculated [32] to be $\gtrsim 5.4$ Å, based on an unresolved line broadening of 0.18 G determined by computer line shape simulation [21].

The formyl radical was conclusively identified in certain X-irradiated Type-III silicas on the basis of its ESR spectroscopy [17]. Even more clearly than for the case of E'_β, the formyl radical is seen in fig. 1 to be created by the reaction of a diamagnetic precursor structure with radiolytic atomic hydrogen which is mobilized at temperatures ~ 130 K. Thus the initial production mechanism was proposed to be [17]

$$H^\circ + CO \overset{130\,K}{\rightarrow} HCO, \tag{5}$$

where the carbon monoxide precursor was inferred to be dissolved in small quantities ($\lesssim 0.1$ ppm) in those Type-III fused silicas which were hydrolyzed in hydrocarbon–oxygen flames. Suprasil and Dynasil evidently fall into this category, whereas Spectrosil – which does not exhibit the formyl radical – is presumed to have been hydrolyzed in a pure H_2–O_2 flame [17].

The formyl radical *per se* may turn out to be no more than a curiosity in the encyclopedia of fused silica. Its optical absorption spectrum in the solid state is still not known, so its influence on the rad hardness of silica-based fiber optics is yet to be assessed. But in terms of divining the mechanisms of defect formation and decay in X-irradiated a-SiO_2 : OH, its discovery looms as a veritable Rosetta stone: The second-stage growth in formyl radical population (by a nontrivial factor of 4) on warming between 170 and 270 K can only be attributed to the reaction of the additional carbon monoxide with additional hydrogen. Since all *atomic* hydrogen was observed directly to disappear above 130 K (fig. 1), a source of additional hydrogen which mobilizes around 230 K is implied.

The nature of the additional (nonparamagnetic) hydrogen is not difficult to infer given the quantitative character of the data of fig. 1. It can be noted that the initial radiolytic yield of H° exceeds by a factor of ~ 2 that of all other defects combined. Thus, even accounting for the reactions of eqs. (4) and (5) and the back reaction of eq. (1), a substantial amount of hydrogen is available for dimerization:

$$2\,H^\circ \overset{130\,K}{\rightarrow} H_2. \tag{6}$$

It was suggested in ref. [17] that this radiolytic molecular hydrogen is immobile in the glass network below 170 K but that above this temperature it begins to move, leading to a series of diffusion-limited reactions initiated by eq. (2). That is, the radiolytic molecular hydrogen reacts with the OHC to produce hydroxyl and an equal number of atomic hydrogens, * the latter reacting in turn with E'_β precursors and CO (when present) to produce E'_β centers and formyl radicals, respectively.

* Presumably the H° released above 200 K is too short lived for ESR observation. However, no concerted search for a transient H° spectrum has yet been made in this temperature regime.

3. The equation

It has been proposed in the preceding sections that diffusion-limited reactions with molecular hydrogen are directly or indirectly responsible for the defect thermal bleaching behaviors above 170 K epitomized in fig. 1. In order to test this propositon it is necessary to compare the data with theoretical predictions based on an appropriate chemical rate theory and thence to compare the parameterization of this theory with published data for the diffusivity of hydrogen in silica.

What constitutes an "appropriate" chemical rate theory can be debated, as many treatments of diffusion-limited reaction kinetics appear in the literature (see, e.g. ref. [33] and references therein). Certainly, the theory of Simpson and Sosin [33] is the most comprehensive, taking explicit account of a number of conceivable situations including the case of correlated defect pairs (e.g., vacancy–intersitial pairs). By constrast, the earlier treatment of Waite [29] was based on the assumption of a uniform initial distribution of reactants. In the examples considered by Simpson and Sosin, a rapid recombination of interstitials with their original vacancies usually accounts for 50–70% of the total recovery [33], with the remaining recombination due to randomly distributed reactants following on a longer time scale. The Waite theory [29] essentially treats only the second of these two substages.

Which theory is correct in the present situation? Simpson and Sosin [33] have pointed out that, when the characteristic diffusion length $(Dt)^{1/2}$ becomes much larger than the capture radius r^*, the probability for an interstitial to escape the environs of its original vacancy becomes significant and the chance encounter of the interstitial with another vacancy or isolated impurity becomes appreciable. Thus, in the event that $(Dt)^{1/2} \gg r^*$, a full diffusional treatment such as that of Waite [29] becomes appropriate. Assuming the diffusivity of hydrogen in silica is accurately expressible as an Arrhenius relation

$$D = D_0 \exp[-E/kT], \tag{7}$$

and taking the values of the preexponential factor and activation energy to be those given by Lee [31] ($D_0 = 5.65 \times 10^{-4}$ cm^2/s, $E = 0.45$ eV), one calculates $(Dt)^{1/2} \gtrsim 500$ Å for typical temperatures and times involved in the experiment of fig. 1. Moreover, the results of isothermal anneal experiments to be presented in section 4 show that no more than 30% of the defects bleach at 235 K in the shortest experimental times, ~ 10 s, for which $(Dt)^{1/2} \sim 200$ Å. Since r^* is reasonably expected to be ~ 5 Å [12,34,35], Waite's formalism seems therefore to be indicated for any analyses of the present data.

But beyond this rough numerical justification for using the Waite approach, an argument can be made to the effect that the initial distribution of H_2 molecules in the glass should in fact be random and uncorrelated with the OHCs: Even assuming that OHCs and H°s might be correlated when originally produced at 77 K, warming above 130 K apparently causes the H°s to diffuse far enough to dimerize [eq. (6)]. Therefore, by 130 K the hydrogen must

have made good its escape from the immediate vicinity of the OHC (or immediate recombination would have occurred) and no further spatial correlations should then exist between the H_2 molecules and the OHCs.

Waite's treatment of bimolecular recombination kinetics in solids is simply presented as a differential rate equation [29]

$$\frac{d[A]}{dt} = \frac{d[B]}{dt} = -4\pi r^* D[A][B]\left\{1 + \frac{r^*}{(\pi Dt)^{1/2}}\right\}, \tag{8}$$

where the concentrations of reactants A and B are represented in square brackets, r^* is the capture radius previously mentioned, and D is the diffusion coefficient of the mobile reactant, as expressed in eq. (7). In the following treatment D_0 of eq. (7) will be regarded as a constant independent of temperature. * The form of eq. (8) is relatively intuitive, except for the second term inside the curly brackets which approximates the recombination behavior of those reactants which are initially inside the capture radius r^* [29].

For the case that the reactants A and B are present in identical concentrations, eq. (8) integrates to [29]

$$\frac{[A]}{[A]_0} = \frac{1}{1 + 4\pi r^* D[A]_0\left(1 + \frac{2r^*}{(\pi Dt)^{1/2}}\right)t}, \tag{9}$$

where $[A]_0$ is the initial concentration of A and, of course, $[B] = [A]$. In the more general situation where $[B] \neq [A]$, integration of eq. (8) yields [29]

$$\frac{[A]}{[A]_0} = \frac{([A]_0 - [B]_0)}{[A]_0 - [B]_0 \exp\left\{-4\pi r^* D([A]_0 - [B]_0)\left[1 + \frac{2r^*}{(\pi Dt)^{1/2}}\right]t\right\}}, \tag{10}$$

where $[B]_0$ is the initial concentration of B. An expression for $[B]/[B]_0$ can be obtained from eq. (10) by permuting the As and Bs inside the square brackets. In general, eq. (10) is sufficient for any practical application, since the behavior described by eq. (9) can be reproduced to any required precision by making $([A]_0 - [B]_0)$ sufficiently small.

4. Curve fitting

Reiterating the central premise of this paper, it is proposed that the thermal bleaching of the OHC above 170 K (fig. 1) is due to a diffusion-limited

* The possibility that D_0 may depend linearly on T has been considered, e.g. refs. [34–36]. However, it has been determined in the course of the present study that the inclusion of such a temperature dependent factor has negligible influence on the quality of the fits achieved in section 4.

reaction with molecular hydrogen [eq. (2)]. To test this notion, the OHC isochronal anneal data of fig. 1 have been normalized to the value recorded following the 150 K anneal step and reproduced in all four panels of fig. 2, where comparisons are made with the predicted behaviors for various parameterizations of eq. (10).

Some of the parameters in eq. (10) were held fixed for all of the calculated

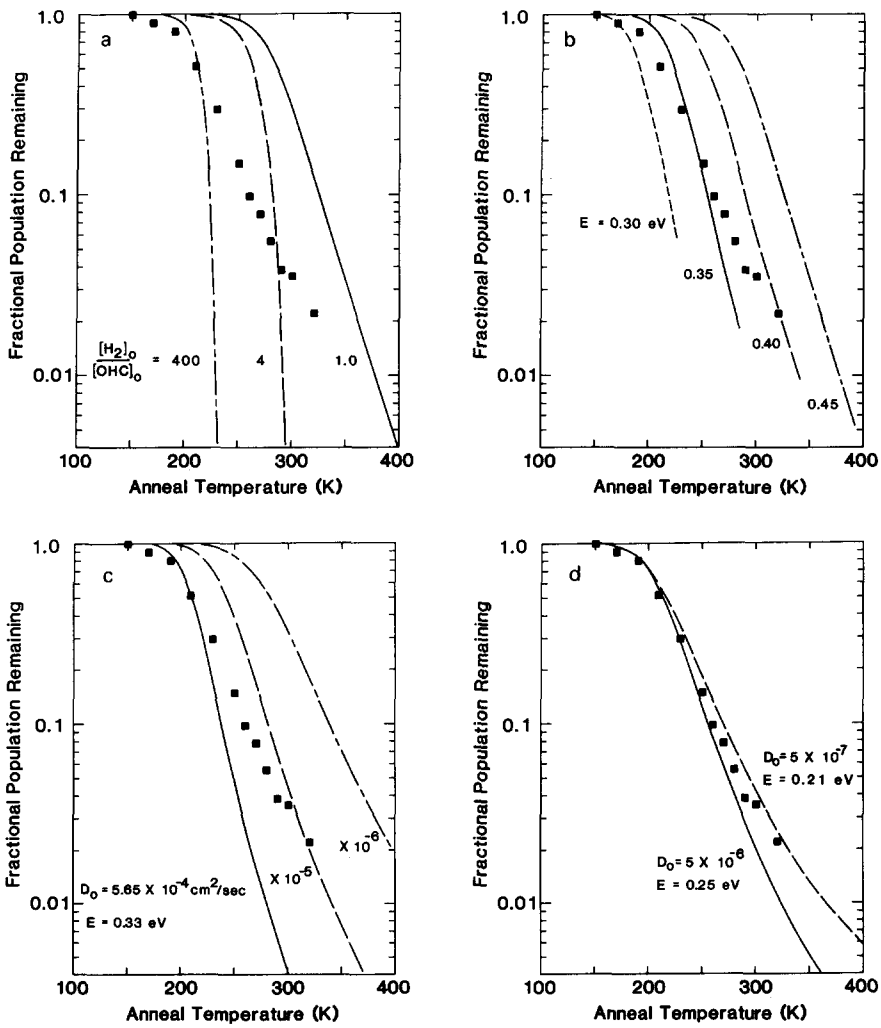

Fig. 2. Isochronal anneal curves for the nonbridging oxygen hole center (OHC) in X-irradiated Suprasil 1. Data points taken from fig. 1 are renormalized to the point at 150 K. Curves are calculated for various parameterizations of eq. (10), assuming the anneal mechanism to be that of eq. (2): (a) effect of varying the initial reactant ratio; (b) effect of varying the activation energy; (c) effect of varying the pre-exponential factor; (d) two attempts at fitting the data by varying both D_0 and E.

curves of fig. 2. These were the capture radius ($r^* = 5$ Å), the time at temperature ($t = 250$ s, assuming a 50 s warmup time), and the "initial" OHC concentration ($[OHC]_0 = 8 \times 10^{14}$ cm^{-3}) measured by ESR following the 150 K anneal step. The calculated anneal curves of fig. 2a incorporate the activation energy E and preexponential factor D_0 given by Lee [31] for hydrogen diffusion in silica.

Several values for the initial ($T = 150$ K) concentration of H_2 were tried in fig. 2a. It can be seen that by assuming $[H_2]_0/[OHC]_0 = 400$ the calculated curve can be made approach the data at the earlier stages of the anneal. However, for values of $[H_2]_0/[OHC]_0 \gtrsim 4$ the calculated curves drop off much too steeply in relation to the data. Moreover, if one assumes with the author that the source of radiolytic H_2 is the dimerization of the "excess" H^0 observed at 100 K (fig. 1), then it fillows that $[H_2]_0/[OHC]_0$ must be $\lesssim 2$ and probably ≈ 1 (realizing that some of the H^0 reacts to form E'_β centers and formyl radicals).

Assuming $[H_2]_0/[OHC]_0 \approx 1$, the theoretically calculated anneal curves can be brought into better coincidence with the data only by lowering the values of E and D_0 below those given by Lee [31]. Fig. 2b shows the effect of lowering the activation energy while holding D_0 fixed at the value given by Lee [31]. On the other hand, fig. 2c explores the influence of lowering the preexponential factor while maintaining a fixed value of E. Finally, fig. 2d illustrates the kinds of fits to the isochronal anneal data which can be achieved by allowing both D_0 and E to vary freely. It should be apparent from fig. 2d that D_0 and E cannot be simultaneously determined to high precision from fits of the isochronal anneal data alone. That is, the good fit achieved by setting $D_0 = 5 \times 10^{-6}$ cm^2/s and $E = 0.25$ eV can be nearly duplicated by lowering D_0 by another order of magnitude while simultaneously decrementing E by ~ 0.05 eV.

Eq. (10) was also used in an attempt to fit a set of *isothermal* anneal data obtained by first warming a sample of Suprasil 1 for 5 min at 130 K (to remove the atomic hydrogen and establish a baseline value for $[OHC]_0$) and then annealing for increasing cumulative times at $T_{anneal} = 235$ K with remeasurement at 100 K. These results are displayed in fig. 3, where the calculated curves are for $D_0 = 5 \times 10^{-6}$ cm^2/s, $E = 0.25$ eV, and various trial values of the initial reactant ratio $[H_2]_0/[OHC]_0$.

Perhaps the most striking feature of fig. 3 is the fact that the calculated behavior for $[H_2]_0/[OHC]_0 = 1.0$ (unbroken curve) fits the data only for $t \approx 250$ s, corresponding to the isochronal anneal time employed in fig. 2. Of course, agreement at this value of t is to be expected, since the values of D_0 and E employed in calculating the curves of fig. 3 where the same as those which yielded the best fit of the data in fig. 2d. But what, then, could be the cause(s) of the discrepancies between theory and experiment at times both much less and much greater than 250 s?

In the long-time regime, it is readily possible that some of the radiolytic H_2 fails to recombine with the OHCs due to percolation bottlenecks (see section 6) or momentary trapping at other sites. Assuming that $\sim 10\%$ of the H_2 is lost to

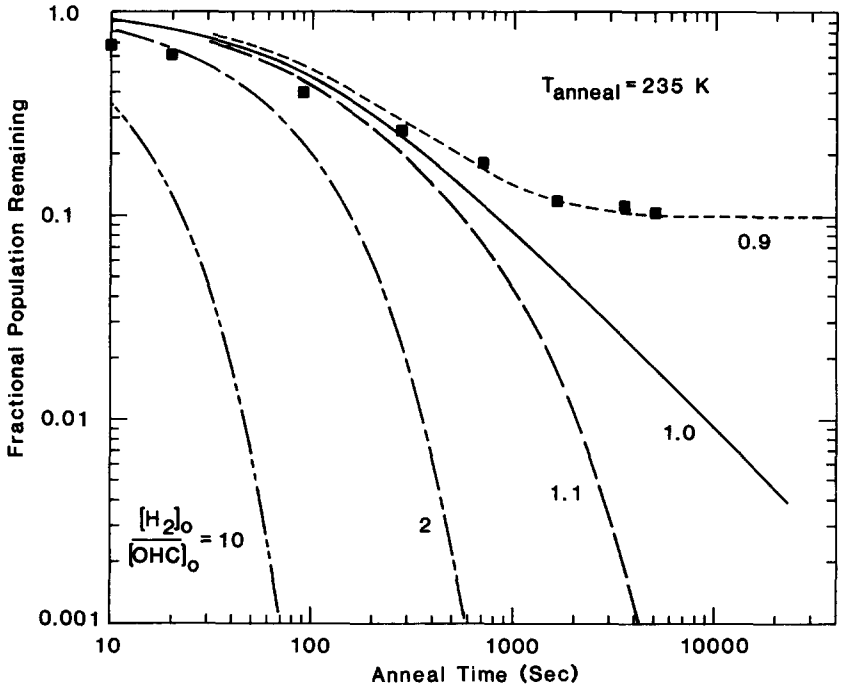

Fig. 3. Isothermal anneal data for the OHC in Suprasil 1 (squares) with comparison to predicted behaviors based on eq. (10) (curves). Sample was X-irradiated at 77 K to a dose of 2×10^6 rad, warmed for 5 min at 130 K to establish the "initial" OHC concentration $[OHC]_0$, and subsequently annealed *in situ* for the indicated lengths of time at 235 K. See text for a discussion of the calculated curves.

such processes, the effect can be approximated by setting $[H_2]_0/[OHC]_0 = 0.9$ (short dashed curve in fig. 3). However, there would seem to be no such "easy" explanation of the discrepancy between theory and experiment at shorter times: Reducing E or increasing D_0 could improve the fit at shorter times but would then introduce a discrepancy in the intermediate time regime. * Moreover, such a change in parameterization would seriously degrade the fits of the isochronal anneal data achieved in fig. 2d.

One possible way out of this dilemma is provided by the possible existence of a *distribution* in activation energies (as proposed in ref. [36]). Fig. 4a displays a composite isochronal anneal curve (dashed curve) generated as a sum of five individual solutions of eq. (10) weighted according to the Gaussian function

* For the values of D_0, E, T, t and r^* presently employed, the term $2r^*/(\pi Dt)^{1/2}$ in eq. (10) takes on values < 0.01 and hence could be safely ignored. To this approximation, the calculated curves of fig. 3 are essentially "universal" in the sense that a change in any one of these parameters would merely translate the entire family of curves forward or backward in time without changing their shapes or relative positions. [For completeness, however, all calculated curves displayed in this paper were generated from eq. (10) without making this approximation.]

shown in the inset. For comparison, the solution for a unique activation energy equal to the mean value of the Gaussian ($E = 0.35$ eV) is shown as the unbroken curve in fig. 4a. A good fit to the experimental data was obtained as

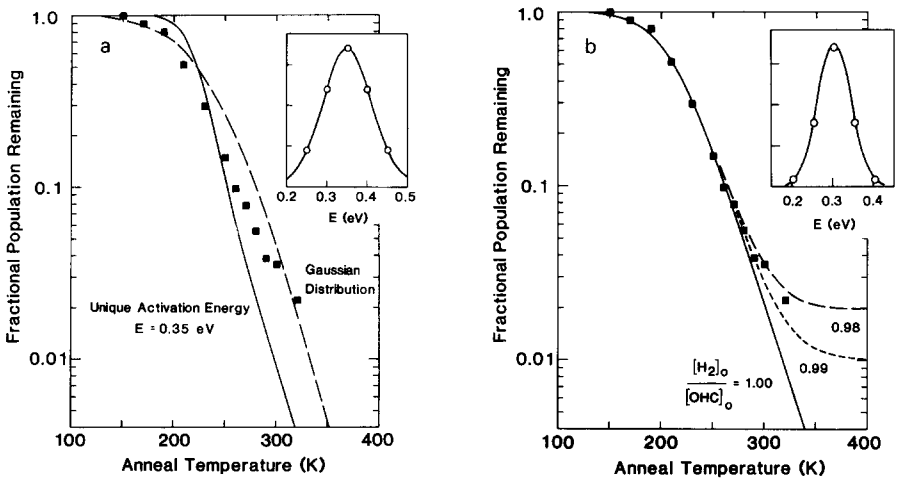

Fig. 4. Isochronal anneal data for the OHC in Suprasil 1 (data points from fig. 2) with comparison to predicted behaviors based on eq. (10) (curves). See text for a discussion of the calculations, including the introduction of the indicated Gaussian distributions in activation energies (insets). A value of $D_0 = 1.5 \times 10^{-4}$ cm^2/s was assumed for the calculations of (b).

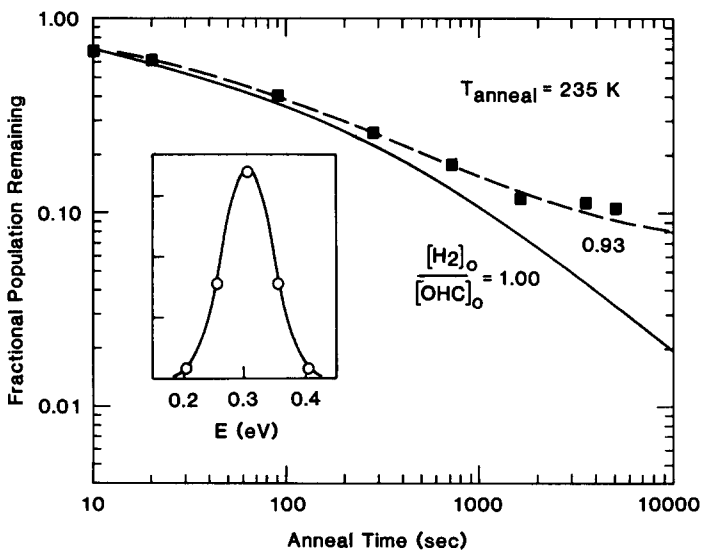

Fig. 5. Isothermal anneal data for the OHC in Suprasil 1 (same data as in fig. 3) with comparison to predicted behaviors based on eq. (10) (curves), assuming the same Gaussian distribution in activation energies (inset) as was employed in the fits of fig. 4b. See text for discussion.

illustrated in fig. 4b by slightly reducing the mean value and width of the Gaussian (inset). Here, the $[H_2]_0/[OHC]_0$ ratio was used as an adjusting parameter to fit the high-temperature data points.

Returning to the *isothermal* anneal problem, the trial distribution of activation energies of fig. 4b was utilized to generate the unbroken curve of fig. 5 *with no further adjustment of parameters* (the data points of fig. 5 are the same as those of fig. 3). By analogy with the procedure used in fig. 4, five separate solutions of eq. (10) were summed according to the indicated weighting factors to generate the calculated curves presented in fig. 5. Again, it was found necessary to use the $[H_2]_0/[OHC]_0$ ratio as a parameter to fit the data at long times; possible justifications for this practice will be considered at greater length in section 7.

5. The diffusion problem

The curve fitting presented above, if meaningful, has implications impinging on the current understanding of hydrogen diffusion in silica and perhaps on the theory of molecular diffusion in glass in general. The present section weighs the results obtained here against the background of previous studies of gas diffusion in glassy silica.

Experimental studies of gas diffusion in glass generally lead to the measurement of diffusivities which when fit to the Arrhenius equation [eq. (7)] lead to values of D_0 and E which are generally increasing functions of the temperature range of the experiment [37]. That is, a plot of the logarithm of diffusivity versus reciprocal temperature differs slightly from a straight line, exhibiting a curvature which is concave upward. Many explanations for this outcome have been considered, most commonly resulting in the suggestion that the preexponential factor should depend on temperature as T^N where N is either $\frac{1}{2}$ or 1 (see, e.g. refs. [34–36]). However, Shelby and Keeton [36] have proposed a model generally more satisfying to one's intuition regarding the randomized structure of glass: namely, it was suggested that the distribution of interstitial sizes and shapes which exist in glasses should give rise to a statistical distribution in activation energies for diffusive motion [36].

Shelby and Keeton [36] developed a formalism for describing the temperature dependence of the measured diffusivity in the event that the activation energy is subject to such a statistical distribution:

$$D = D_0 \exp(\sigma^2/4k^2T^2) \exp(-\epsilon/kT), \tag{11}$$

where ϵ and σ $(\ln 2)^{1/2}$ are the mean value and half-width-at-half-maximum, respectively, of a Gaussian distribution of activation energies. Eq. (11) is an approximation which is reasonably valid for $\epsilon - \sigma^2/2kT > 3\sigma$ [36]. Shelby and Keeton went on to show that a large body of data [38] for the diffusivity of He in a-SiO_2 could be fit by eq. (11) by taking $\epsilon \approx 0.33$ eV and $\sigma \approx 0.081$ eV.

Fig. 6 provides a graphic representation of the diffusivity of He in silica

versus reciprocal temperature using the above parameterization of eq. (11) (boldly drawn curve). Here, the lightly drawn rays eminating from the infinite-temperature intercept correspond to the five activation energy values denoted by circles on the probability distribution function suggested by Shelby and Keeton [36] (inset). The dashed curve in fig. 6 is an "average diffusivity" crudely calculated as a sum of the diffusivities represented by the five rays, weighted according to the distribution function of the inset. The general agreement between the bold and dashed curves suggests that such a crude 5-point average can reasonably approximate the effects of the postulated distribution in activation energies.

Of course, if an "average diffusivity" is all that is desired, then the Shelby–Keeton formalism [eq. (11)] is much to be preferred over a crude

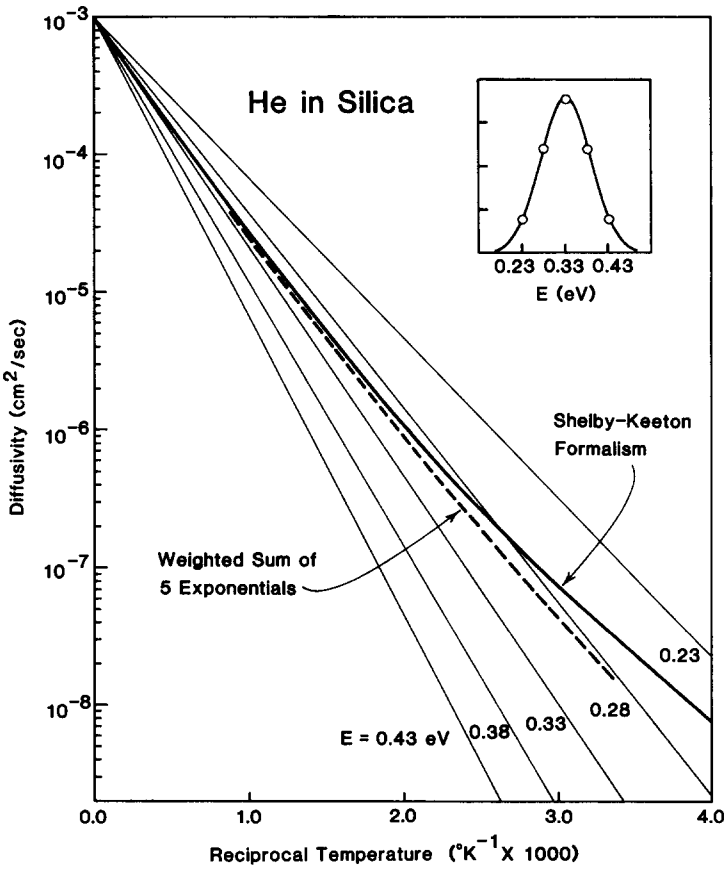

Fig. 6. Diffusivity of He in fused silica as a function of reciprocal temperature. The bold unbroken curve is calculated by means of eq. (11) using the distribution in activation energies (inset) and pre-exponential factor determined by Shelby and Keeton [36] to fit the available experimental data (not shown). Lightly drawn straight lines represent hypothetical diffusivities for five discrete activation energies, assuming the same pre-exponential factor.

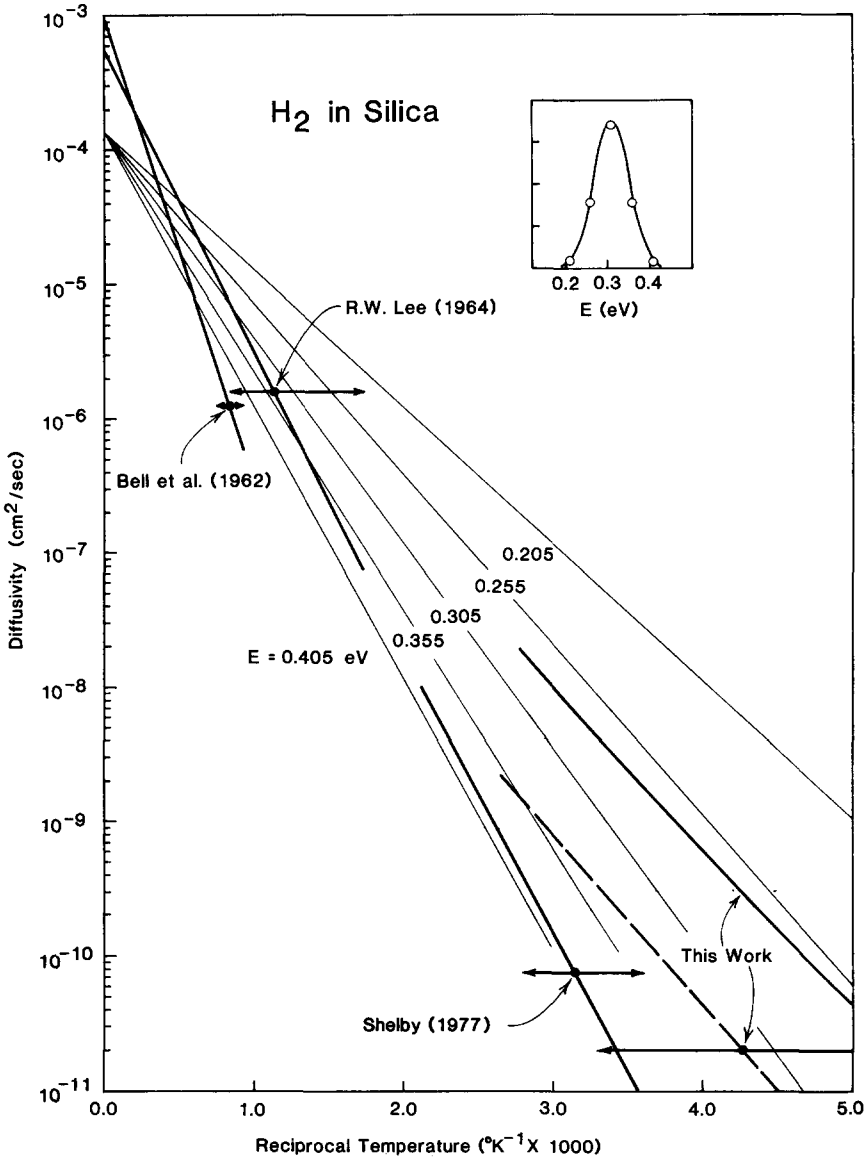

Fig. 7. Diffusivity of H_2 in fused silica as a function of reciprocal temperature. The results of Bell et al. [39], Lee [31] and Shelby [40] are expressed as simple Arrhenius relations (bold straight lines on this plot). The results of the present work from the fits of figs. 4b and 5 are calculated by means of eq. (11) (bold curve) using the indicated distribution in activation energies. The best "nondistributed parameter" fit from fig. 2d is represented as the bold dashed line. Lightly drawn rays are analogous to those defined in fig. 6. Horizontal arrows delineate the temperature ranges of the respective experiments and the measured diffusivity at the midpoint of these temperature ranges (filled circles). Discrepancies among the various sets of experimental results are discussed in the text.

average. But herein lies an important point to be emphasized: The curve fits of figs. 4 and 5 could not have been achieved by simply substituting the average values of D given by eq. (11) back into eq. (10). Rather, these fits were only accomplished by calculating weighted sums of the solutions of eq. (10) for a range of activation energies. The implications of this fact may be profound. For if the present procedure is meaningful, it must be concluded that the diffusing species (H_2 in the present experiment) does not make enough hops before reacting with an OHC to sample the full range of activation energies and thereby to be characterized by an "average diffusivity." Rather, it would follow that each H_2 molecule samples a pathway characterized by an activation energy generally different from those of the pathways sampled by others of the diffusing H_2 species; this aspect of the problem will be discussed at greater length in sections 6 and 7.

In any event, it is informative to compare the H_2 diffusivities determined in the present experiment with the values to be found in the literature [31,39,40]. This has been done in fig. 7, where eq. (11) has been used to generate an "average diffusivity" from the Gaussian distribution in activation energies used in the fits of figs. 4 and 5. It can be seen that the latter curve does not join smoothly with the Arrhenius relationships determined by Lee [31] and Shelby [40] and disagrees even more dramatically with the results of Bell et al. [39]. Possible reasons for the discrepancy between the results of refs. [31] and [39] have been discussed by Lee [31] and will be treated at greater length in section 8. The following section will deal with the thornier problem of the discrepancy seen in fig. 7 between the results of Lee [31] and Shelby [40] and those of the present work.

6. H_2 Diffusion at cryogenic temperatures: a percolation problem

In fig. 7, Shelby's results for D_2 diffusion [40] when multiplied by an anticipated isotope effect factor of $2^{1/2}$ [41] are seen to be in excellent agreement with an extrapolation of the results of Lee [31] for the diffusion of H_2 at higher temperatures. Therefore the present results for H_2 diffusivity below room temperature are clearly discrepant with the macroscopic average diffusivities measured in the temperature ranges 278–360 K [40] and 570–1270 K [31]. That this disagreement is not merely related to the assumption of a Gaussian distribution in activation energies in the analyses of figs. 4 and 5 is apparent from the results of one of the "nondistributed parameter" fits of fig. 2d, portrayed as the dashed straight line in fig. 7. It is clear then that the present experiment is probing a diffusive phenomenon qualitatively different from that which is measured in more classical studies, such as those involving evolution of dissolved gas from a membrane, e.g., [31,35,40].

A potential understanding of why the present results should differ from those of the more traditional approaches is evinced in fig. 8. Here, a measure of the rms diffusion length $(\pi Dt)^{1/2}$, is plotted versus time at 235 K for a range

of activation energies encompassing the trial distribution function of figs. 4 and 5, as well as the macroscopic average value of 0.45 eV determined for hydrogen isotope diffusion in silica by Lee [31] and Shelby [40]. Also shown in the figure as curve A is the average distance between defect centers (OHC population)$^{-1/3}$ for a silica sample which had received an X-ray dose of $\sim 1.5 \times 10^6$ rad (as in fig. 1). It is significant to note that an H_2 molecule diffusing in a pathway characterized by the average activation energy of 0.45 eV will not traverse the mean distance between centers in typical experimental times! Assuming that H_2 is indeed the diffusing species (as is supported by abundant data and arguments presented in sections 1, 2, and 8), *the existence within the glass of diffusion pathways with lower-than-average activation energies is clearly required to explain the observed thermal bleaching of OHCs.*

Percolation theory is the embodiment of the concept that diffusion of a particulate fluid through a randomized solid should be controlled both by the availability of open solubility sites and by the probability that a given open site is part of a connected cluster of sites (or "pathway") of sufficient length.

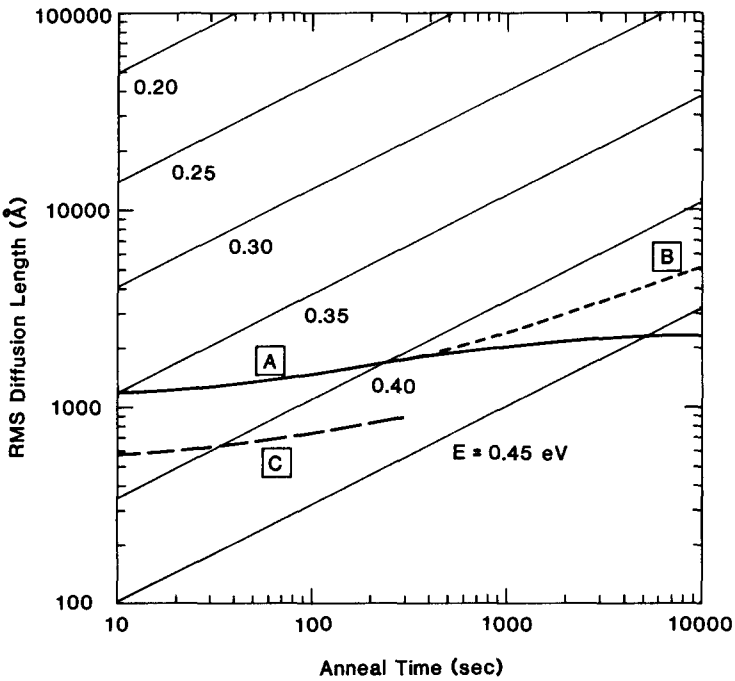

Fig. 8. Theoretical rms diffusion lengths $(\pi Dt)^{1/2}$ (straight lines) versus anneal time t, assuming $D = D_0 \exp(-E/kT)$, where $D_0 = 1.5 \times 10^{-4}$ cm^2/s and $T = 235$ K, for various values of the activation energy E. Curve A represents the mean distance between defect centers $[OHC]^{-1/3}$ using the data of fig. 3, where $[OHC]_0 \approx 8 \times 10^{14}$ cm^{-3}. Curve B is the predicted behavior based on eq. (9). Curve C indicates the initial mean distance between centers when $[OHC]_0 \approx 5 \times 10^{15}$ cm^{-3}.

Brandt [42,43] has performed percolation theory calculations for several ordered and random arrays and made comparisons with data for rare gas solubilities and diffusivities in fused silica. On the basis of these comparisons he proposed "that in the glass structure the various gas molecules may find and utilize certain useful diffusion paths, perhaps connected defect clusters or disorganized regions of low density, and that other regions of higher order and compactness remain practically impermeable to, and are bypassed by, the migrating species." In the present context, only a few comments need be added: First, there must exist far more pathways of ~ 1000 Å average lengths (as needed for the thermal bleaching of OHCs by H_2 diffusion) than pathways of ~ 0.1 mm lengths (as required for typical gas evolution measurements, e.g., ref. [40]). Second, as shorter and shorter pathways are considered the probability must become higher and higher of encountering pathways characterized by activation energies differing from the macroscopic average. Finally, while it is undoubtedly the case that the vast majority of all 1000 Å pathways must be characterized by the macroscopic average diffusity, reference to fig. 8 shows that these (more numerous) high-energy pathways would be frozen out and effectively "short circuited" by any lower energy pathways which may exist in the sample.

While the picture sketched above seems cogent, some further tests of its predictions are desirable. One such prediction flows from fig. 8: if the concentration of defects is increased, the average distance between defect centers will decrease and, as a consequence, some of the (more numerous) higher-energy pathways should contribute to the thermal bleaching process. In other words, the mean activation energy measured in the experiment might be

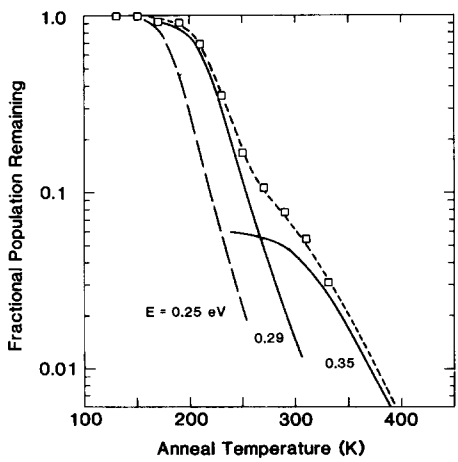

Fig. 9. Isochronal anneal curves for the nonbridging oxygen hole center in Suprasil 1 irradiated to a dose of 8.5×10^6 rad 100 keV X-rays. Data points taken from ref. [17] are renormalized to the point at 150 K. Unbroken and long-dashed curves were calculated from eq. (9) using $D_0 = 5 \times 10^{-6}$ cm^2/s, and the indicated values of E. Short-dashed curve is the sum of the unbroken curves.

higher for higher defect concentrations. That this actually seems out to be the case experimentally is seen in fig. 9. Here, the data points pertain to a sample of Suprasil 1 exposed to 8.5×10^6 rad 100 keV X-rays (about six times the dose of the samples of figs. 1–5) and containing an OHC population at 150 K of $\sim 5 \times 10^{15}$ cm^{-3} (or about six times the OHC concentration of figs. 1–5) [17]. For reference, the long dashed curve in fig. 9 was calculated using the same values of D_0 ($= 5 \times 10^{-6}$ cm^2/s) and E ($= 0.25$ eV) as provided the best "nondistributed parameter" fit of fig. 2d, under the usual assumption that $[H_2]_0 = [OHC]_0$. On the other hand, the unbroken curve exhibiting the best fit to the low temperature data of fig. 9 employed the same value of D_0 but $E = 0.29$ eV. Finally, the unbroken curve multiplied by a scale factor of 0.06 and approximating the behavior of the high-temperature data points was calculated using $E = 0.35$ eV (and assuming $[H_2]_0 = [OHC]_0 = 0.06 \times 5 \times 10^{15}$ cm^{-3}). Thus, an increase in defect concentration by a factor of six is seen to result in an increase in the measured mean value of E from 0.25 to 0.29 eV (with $\sim 6\%$ of the centers showing a still higher activation energy of 0.35 eV). This finding provides intriguing support for the present view that short range diffusion of H_2 in silica glass at cryogenic temperatures must find its description in percolation theory.

7. Interpretation of the curve fitting results

It is clear that the Gaussian distribution of activation energies used to fit the data sequences of figs. 4b and 5 cannot represent the true distribution of activation energies for H_2 jumps in silica, since this distribution does not encompass the mean activation energy of 0.45 eV known from classical gas evolution studies [31,40]. Furthermore, accepting the percolation interpretation of section 6, it must be recognized from fig. 8 that those short circuit pathways with lower mean activation energies are characterized by longer diffusion lengths per unit time and hence must contribute to the bleaching process well out of proportion to the absolute numbers of these pathways available. In other words, the trial distribution functions of figs. 4 and 5 probably represent the *product* of the activation energy distribution over available pathways *times* the rms diffusion length as a function of activation energy. This "effective" distribution would be abruptly truncated, however, when as function of increasing energy the rms diffusion length drops below the mean separation between defect centers. This proposed interpretation of the distribution functions determined by curve fitting is illustrated in fig. 10.

The present percolation picture also affords a reasonable explanation for the need to employ the initial reactant ration $[H_2]_0/[OHC]_0$ as an adjustable parameter in figs. 3–5. For example in fig. 5, setting $[H_2]_0/[OHC]_0 = 0.93$ is tantamount to assuming that $\sim 7\%$ of the radiolytic hydrogens are unable to access short circuit paths to the remaining OHCs for $T = 235$ K and experimental times $\lesssim 5000$ s. On the other hand, raising the temperature (as in the

isochronal anneal experiment of fig. 4b) makes higher energy pathways available, thus reducing to ~ 1% the amounts of residual reactants by the conclusion of the experiment. The curve fitting of fig. 9 suggests, however, that at higher X-ray doses a subpopulation of defects is formed (~ 6% of the total) in sites which are relatively impervious to diffusing H_2 molecules except via relatively high energy pathways ($E \approx 0.35$ eV).

8. Chemical effects

The interpretations offered so far have involved physical diffusion of molecular H_2 through the a-SiO_2 network without chemical reaction beyond that which effects the ultimate thermal bleaching of the defects, eq. (2). Lee [31] and, particularly, Shelby [40] carefully illustrated the fact that reactionless diffusion can be observed in classical diffusion measurements even at higher temperatures in high-OH Type-III silicas, with an activation energy of E_m = 0.45 eV. Lee [31] argued convincingly that the higher activation energy reported by Bell et al. [39] ($E_d = 0.69$ eV) must be due to "the conversion of metastable hydroxyl to molecular hydrogen," resulting in "an internal source of diffusable gas." It is suggested here that the specific reaction responsible for

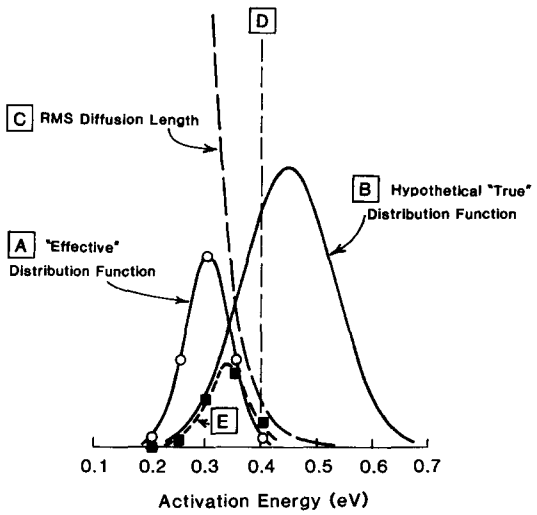

Fig. 10. Proposed relationship between the "effective" distribution in activation energies (A) for H_2 diffusion determined by the curve fitting of figs. 4b and 5 and the hypothetical "true" distribution in activation energies (B). Curve A is suggested to be given by Curve B multiplied by the rms diffusion lenght (C) as modified by an abrupt cutoff at energies above the "freeze out" energy (D) (see fig. 8). Thus, the result (E) of dividing curve A by curve C should reproduce curve B only at energies sufficiently below the freeze out energy D. Curve B, a Gaussian centered at the macroscopic average activation energy, was constructed to yield this agreement.

the additional diffusable H_2 measured by Bell et al. [39] must be *

$$\equiv \mathrm{Si{-}OH\ HO{-}Si} \equiv \rightleftharpoons \equiv \mathrm{Si{-}O{-}O{-}Si} \equiv + H_2. \tag{12}$$

Eq. (12) is in fact the process tentatively proposed by Shelby [41] for the reaction of hydrogen with hydroxyl-free fused silica. Shelby suggested this reaction because of its consistency with several experimental facts, including (a) observation of the peroxy radical defect in heavily irradiated fused silicas [47] and in low-OH fused silicas following fiber drawing [13,48], (b) the occurrence of hydroxyl but not hydride when hydrogen is reacted with low-OH silicas [41], and (c) the limited number of reaction sites ($\sim 3 \times 10^{18}$ cm^{-3}) implied by the saturation yield of hydroxyl groups in Suprasil W-1 [41]. Shelby [41] emphasized, however, that the activation energy of 0.29 eV determined in his permeation experiment was controlled by the diffusion of hydrogen molecules and therefore tells nothing about the reaction of eq. (12) itself. That is, when H_2 is permeated into a low-OH silica the reaction of eq. (12) proceeds to the left with diffusion-limited kinetics, at least for temperatures down to 773 K [41].

Assuming this model, the equilibrium concentration of dissolved hydrogen $[H_2]$ can be expressed in terms of the concentration of *metastable* + OH^- groups $[OH^-]_{meta}$ and the concentration of peroxy linkages $[O_2^{2-}]$:

$$\frac{[H_2][O_2^{2-}]}{[OH^-]^2_{meta}} = K = \exp\left(-\frac{E_s}{kT}\right), \tag{13}$$

where E_s is related to the measured activation energies for diffusion with and without reaction (E_d and E_m, respectively) according to [49]

$$E_d = E_m + E_s/2. \tag{14}$$

If no additional hydrogen is permeated from the outside (and none is extracted), then the intrinsic (equilibrium) dissolved hydrogen content $[H_2]_i$ is equal to the intrinsic peroxy linkage concentration $[O_2^{2-}]_i$ and is given by

$$[H_2]_i = [OH^-]_{meta} \exp(-E_s/2kT). \tag{15}$$

If one accepts from Bell et al. [39] a value of $E_d \approx 0.69$ eV and from Lee [31] and Shelby [40] a value of $E_m \approx 0.45$ eV, then one calculates $E_s \approx 0.48$ eV for

* This reaction has been independently cited by Robertson [44] as the probable explanation of the results of Bell et al. [39]. Moreover, it is also analogous to a process demonstrated to occur when H_2O is dissolved in other insulators such as MgO [45,46].

+ According to Lee [31], most of the OH in fused natural quartz is metastable (removable by gas extraction), whereas the majority of the OH groups in synthetic silicas such as Suprasil 1 are "permanent." Shelby [50] contends, however, that a significant fraction of the hydroxyl groups in Suprasil 1 is metastable. In any event, under the present operating hypothesis, one would presume that the *metastable* OH groups always occur in closely associated pairs.

the activation energy governing the equilibrium constant of eq. (13). Putting the latter value back into eq. (15) and using for $[OH]_{meta}$ twice the number of reaction sites determined by Shelby [41] for Suprasil W-1 leads to a value of $[H_2]_i \approx 4 \times 10^{13}$ cm^{-3} at 235 K. This number is small with respect to the amounts of radiolytic hydrogen inferred to be generated in Suprasil 1 by an X-ray dose of 1.5×10^6 rad, viz., $\sim 8 \times 10^{14}$ cm^{-3} (see section 2), in agreement with an implicit assumption of section 4. However, if the present parameterization of eq. (15) is correct, $[H_2]_i$ would become comparable to the concentration of radiolytic hydrogen at lower doses or higher temperatures.

It is interesting to explore the consequences of upsetting the equilibrium of eq. (12) by extracting hydrogen prior to irradiation. Fig. 11a compares the H° and OHC isochronal anneal data for the stock Suprasil 1 rods of fig. 1 with analogous data for an equivalent sample of the same material which was annealed overnight in air at 1100°C just prior to irradiation and ESR investigation. (Also included in this figure are data for an off-the-shelf 4 mm rod of Spectrosil.)

The most striking feature of fig. 11a is the fact that the 1100°C pretreatment results in the near total suppression of the OHC thermal bleaching step which occurs between ~170 and 300 K for the off-the-shelf samples of

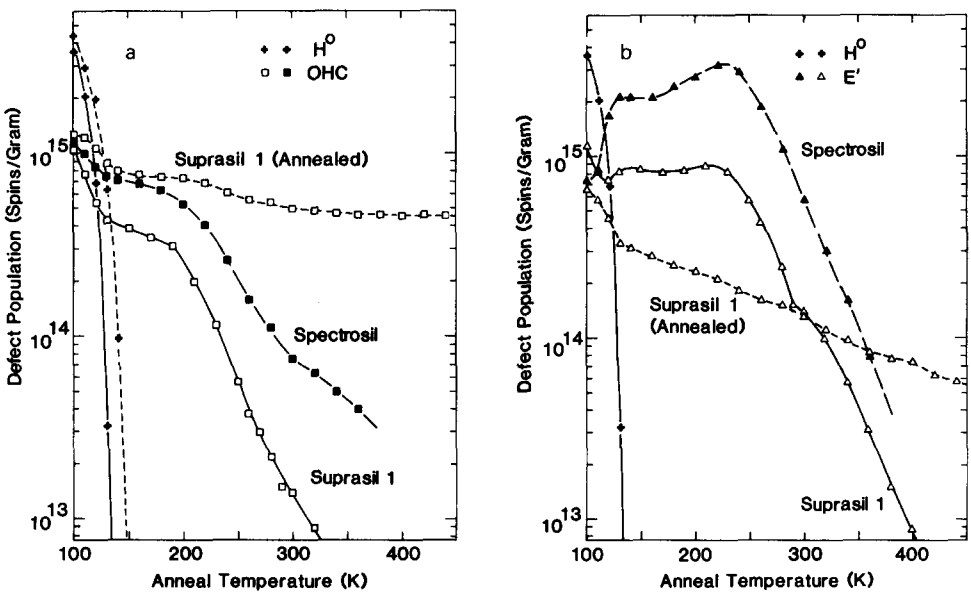

Fig. 11. Comparison of isochronal anneal behaviors of X-ray-induced defect centers in several samples of high purity Type-III fused silicas: (a) H° and OHC, (b) H° and E′ centers. The atomic hydrogen anneal curves for the unheated samples of Suprasil 1 and Spectrosil were virtually identical and are represented by the crosses and unbroken curve; dashed curve in (a) pertains to a sample of Suprasil 1 annealed overnight at 1100°C. Data were obtained as described in the caption to fig. 1.

Suprasil 1. Of course, it is this very bleaching step which is herein attributed to the diffusion-limited reaction of radiolytic H_2 with the OHCs according to eq. (2). Suppression of this process in the pre-annealed sample is quite evidently not due to a deficiency in the initial yield of atomic hydrogen, since as seen in fig. 11a the H° count at 100 K is the same for both the annealed and unannealed samples. One may then infer that the yield of molecular hydrogen due to the dimerization of the H° is probably also the same in both cases.

What then causes the OHCs in the stock Suprasil sample to bleach almost completely by 300 K while those in the 1100 °C-heated sample bleach virtually not at all? The only answer which suggests itself is that the radiolytic H_2 in the heat-treated sample must be gettered by some kind of traps not present in the off-the-shelf sample. Specifically, it is proposed that these traps comprise an excess of peroxy linkages $\equiv Si-O-O-Si \equiv$ left in the sample as a consequence of some of the H_2 on the right hand side of eq. (12) outdiffusing during the 1100 °C heat treatment. In this scenario, most of the radiolytic molecular hydrogen is consumed in an effort to drive the reaction of eq. (12) back to the left. As a result, few of the H_2 molecules are available to react with OHCs according to eq. (2), and the material therefore suffers "permanent" damage rather than damage which slowly fades at room temperature.

Similarly, from the results of fig. 11a it might be suggested that the sample of Spectrosil investigated is substantially more hydrogen deficient than the stock samples of Suprasil 1. However, the data for the *E′ center* bleaching behaviors shown in fig. 11b indicate that the differences between Suprasil and Spectrosil may be more complex than this. The increased E'_β yield for this particular sample of Spectrosil (some samples behave more like Suprasil [17]) suggests a greater concentration of E'_β precursors. At the same time, additional traps seem to have been provided to mitigate the reaction of radiolytic H_2 with the OHCs. An example of an additional process which might conceivably be at work here would be the equilibrium

$$\equiv Si-H\ H-Si \equiv \rightleftharpoons \equiv Si-Si \equiv + H_2, \tag{16}$$

which can be seen to be analogous to eq. (12) if an oxygen vacancy is substituted for the peroxy linkage. In this scheme, the oxygen vacancy serves both as a trapping site for molecular hydrogen and as a precursor for E'_β [21]:

$$\equiv Si-Si \equiv + H^\circ \rightarrow \equiv Si\cdot \quad H-Si \equiv . \tag{17}$$

[Note that eq. (17) is a more structure-specific way of presenting eq. (4).]

If eq. (17) should prove to be the correct model for E'_β, then its anneal mechanism, like that of the OHC, is also likely to be related to hydrogen diffusion. Since E'_β, the OHC, and the formyl radical are the only paramagnetic defects seen at 300 K (figs. 1 and 11), it would follow that all room temperature bleaching – including that observed for the induced attenuation in fiber optic waveguides [8–10] – is probably tied in some way to an H_2 diffusion mechanism.

9. Summary and projections

It has been shown above that the thermal bleaching of *X*-ray-induced nonbridging oxygen hole centers in Type-III fused silicas can be ascribed to a diffusion-limited reaction of these centers with radiolytic molecular hydrogen [Eq. (2)]. That this hydrogen is indeed a product of radiolysis can be inferred from mathematical modeling of the isochronal and isothermal anneal curves which generally requires that $[H_2]_0/[OHC]_0 \sim 1$ (section 4) and from direct ESR observation of sufficient atomic hydrogen to produce these amounts of radiolytic H_2 (fig. 1). Furthermore, the concentration of nonradiolytic hydrogen in the samples has been estimated in section 8 to be lower than the induced OHC populations under present experimental conditions.

Under this working hypothesis, the diffusivity of H_2 in a-SiO_2 has been estimated at cryogenic temperatures and comparisons have been made with published data. The present results are seen to yield substantially higher diffusivities and lower activation energies in the temperature range 150–300 K than predicted by extrapolation of data obtained at higher temperatures by more classical methods (fig. 7). It has been argued in section 6 that this apparent discrepancy can be understood in terms of the existence of a statistical distribution in activation energies (as proposed in ref. [36]): In the language of percolation theory, those diffusion pathways characterized by the average activation energy (high-temperature bulk value) are frozen out in the cryogenic temperature range and are "short circuited" on the distance scale of the present experiment (~ 1000 Å) by less numerous but more efficient pathways on the low-energy tail of the distribution function.

In section 8, the present results have been projected as strongly suggesting that the slow room-temperature fading of radiation-induced attenuation in pure-silica core optical fibers [6–10] may be entirely controlled by the diffusion of radiolytic H_2. It has also been shown in section 8 how this intrinsic radiation protection mechanism can be defeated by processing steps which remove hydrogen from the material prior to its exposure to radiation; indeed, such effects appear to have been observed recently in high-purity silica-core optical fiber waveguides [8]. Still more recent work [51–55] has shown that molecular hydrogen itself when dissolved in silica glass absorbs light in the wavelength windows of interest for optical communications. The present study thus predicts the occurrence of transient radiation-induced optical absorption bands in high-OH silica-core optical fibers due to the production and diffusion-limited back reaction of radiolytic H_2. Finally, it should be mentioned in the present context that recent evidence has been given for OH band formation in hydrogen-permeated doped-silica core optical fibers under conditions of moderate temperature ($\sim 200\,^\circ$C) and stress [52,56]. The latter phenomena may well have their origins in processes analogous to the reverse reaction of eq. (12).

R.J. Ginther is thanked for performing the 1100 °C pretreatment of a

sample described in section 8. The author is also grateful to J.E. Shelby and A.R. Cooper for their helpful comments on the original draft of this manuscript.

References

[1] A.J. Cohen, J. Chem. Phys. 55 (1955) 765.
[2] G.W. Arnold and W.D. Compton, Phys. Rev. 116 (1959) 802.
[3] W.D. Compton and G.W. Arnold, Disc. Faraday Soc. 31 (1961) 130.
[4] E.W.J. Mitchell and E.G.S. Paige, Phil. Mag. 1 (1956) 1085.
[5] R.A. Weeks, Proc. 7th Int. Cong. Glass, paper No. 41, Brussels.
[6] E.J. Friebele and M.E. Gingerich, Appl. Optics 20 (1981) 3448.
[7] E.J. Friebele, M.E. Gingerich and K.J. Long, Appl. Optics 21 (1982) 547.
[8] E.J. Friebele, M.E. Gingerich, K.J. Long, P.S. Levin and D.A. Pinnow, IEEE J. Lightwave Tech. LT-1 (1983) 462.
[9] E.J. Friebele, C.G. Askins, M.E. Gingerich and K.J. Long, Nucl. Instr. and Meth. B1 (1984) 355.
[10] E.J. Friebele and K.J. Long, unpublished data.
[11] E.J. Friebele and D.L. Griscom, Treatise on Materials Science and Technology, Vol. 17, Glass II, eds., M. Tomozawa and R.H. Doremus (Academic Press, New York, 1979) p. 257.
[12] A.H. Edwards and W.B. Fowler, Phys. Rev. B26 (1982) 6649.
[13] M. Stapelbroek, D.L. Griscom, E.J. Friebele and G.H. Sigel Jr, J. Non-Crystalline Solids 32 (1979) 313.
[14] A.G. Revesz, IEEE Trans. Nucl. Sci. NS-18 (1971) 113.
[15] A.R. Silin, L.N. Skuya and A.V. Shendrik, Fiz. Khim, Stekla 4 (1978) 410.
[16] A.R. Silin and L.N. Skuja, J. Mol. Struct. 61 (1980) 145.
[17] D.L. Griscom, M. Stapelbroek and E.J. Friebele, J. Chem. Phys. 78 (1983) 1638.
[18] R.A. Weeks, J. Appl. Phys. 27 (1956) 1376.
[19] D.L. Griscom, Phys. Rev. 20 (1979) 1823.
[20] D.L. Griscom, Phys. Rev. 22 (1980) 4192.
[21] D.L. Griscom, Nucl. Instr. and Meth. B1 (1984) 481.
[22] S.P. Faile, J.J. Schmidt and D.M. Roy, Science 156 (1967) 1593.
[23] S.P. Faile and D.M. Roy, J. Am. Ceram. Soc. 54 (1971) 533.
[24] C.M. Hartwig, J. Chem. Phys. 66 (1977) 227.
[25] J.E. Shelby, J. Appl. Phys. 50 (1979) 3702.
[26] J.E. Shelby, P.L. Mattern and D.K. Ottensen, J. Appl. Phys. 50 (1979) 5533.
[27] J. Vitko Jr, J. Appl. Phys. 49 (1978) 5530.
[28] J.E. Shelby (preprint supplied by author, 1983).
[29] T.R. Waite, Phys. Rev. 107 (1957) 463.
[30] D.L. Baulch, R.A. Cox, R.F. Hampson Jr, J.A. Kerr, J. Troe and R.T. Watson, J. Phys. Chem. Ref. Data 9 (1980) 295.
[31] R.W. Lee, Phys. Chem. Glasses 5 (1964) 35.
[32] D.L. Griscom, J. Non-Crystalline Solids 64 (1984) 229.
[33] H.M. Simpson and A. Sosin, Radiat. Eff. 3 (1970) 1.
[34] R.H. Doremus, in: Modern Aspects of the Vitreous State, ed., J.D. Mackenzie, Vol. 2 (Butterworth, London, 1962) p. 1.
[35] J.E. Shelby, in: Treatise on Materials Science and Technology, Vol. 17, Glass II, eds., M. Tomozawa and R.H. Doremus (Academic Press, New York, 1979) p. 1.
[36] J.E. Shelby and S.C. Keeton, J. Appl. Phys. 45 (1974) 1458.
[37] J.E. Shelby, J. Am. Ceram. Soc. 54 (1971) 125.
[38] J.E. Shelby, J. Am. Ceram. Soc. 55 (1972) 61.
[39] T. Bell, G. Hetherington and K.H. Jack, Phys. Chem. Glasses 3 (1962) 129.
[40] J.E. Shelby, J. Appl. Phys. 48 (1977) 3387.

[41] J.E. Shelby, J. Appl. Phys. 51 (1980) 2589.
[42] W.W. Brandt, J. Chem. Phys. 63 (1975) 5162.
[43] W.W. Brandt, Phys. Stat. Solidi (a)30 (1975) 263.
[44] J. Robertson (submitted to J. Phys. C).
[45] F. Freund, H. Wengeler and R. Martens, Geochim. Cosmochim. Acta 46 (1982) 1821.
[46] F. Freund, H. Wengler, H. Kathrein and R. Knobel, Nucl. Instr. and Meth. B1 (1984) 223.
[47] E.J. Friebele, D.L. Griscom, M. Stapelbroek and R.A. Weeks, Phys. Rev. Lett. 42 (1979) 1346.
[48] E.J. Friebele, G.H. Sigel Jr and D.L. Griscom, Appl. Phys. Lett. 28 (1976) 516.
[49] B. Henderson, Defects in Crystalline Solids (Arnold, London, 1972).
[50] J.E. Shelby (private communication).
[51] J. Stone, A.R. Chraplyvy and C.A. Burrus, Opt. Lett. 7 (1982) 297.
[52] K. Mochizuki, Y. Namihira and H. Yamamoto, Electron, Lett 19 (1983) 743.
[53] N. Uesugi, Y. Murakami, C. Tanaka, Y. Ishida, Y. Mitsunaga, Y. Negishi and N. Uchida, Electron Lett. 19 (1983) 762.
[54] M. Fox and S.J. Stannard-Powel, Electron. Lett. 19 (1983) 916.
[55] K.J. Beales, D.M. Cooper and J.D. Rush, Electron. Lett. 19 (1983) 917.
[56] N. Uesugi, T. Kuwabara, Y. Koyamada, Y. Ishida and N. Uchida, Appl. Phys. Lett. 43 (1983) 327.